symmetry

MDPI

Article

Mechanical Behavior of Secondary Lining in Super Large-Span Tunnels Considering Temperature Effects

Fangfang Dong [1], Yanbin Luo [1,*], Jianxun Chen [1], Chuanwu Wang [1], Yahui Liu [2] and Wenjie Xun [1]

[1] School of Highway, Chang'an University, Xi'an 710064, China; 2017021020@chd.edu.cn (F.D.); chenjx1969@chd.edu.cn (J.C.)
[2] Guangzhou Metro Design & Research Institute Co., Ltd., Guangzhou 510000, China; liuyahui@gmdi.cn
* Correspondence: lyb@chd.edu.cn

Abstract: Temperature stress has a significant impact on the structural stress of (super) large-span tunnel lining, which can easily lead to structural fatigue damage and premature cracking. With the increasing scale and quantity of super large-span tunnels, the issue of temperature stress in secondary lining has attracted widespread attention. Previous studies have paid little attention to the influence of temperature stress on the structural internal forces of ordinary small–medium-span tunnels, but this influence cannot be ignored for super large-span tunnels. We take the Letuan Tunnel (a double-hole eight-lane tunnel) of the Binzhou-Laiwu expressway renovation and expansion project in Shandong Province as a case study and analyze the mechanical response of the secondary lining through on-site measurement. Moreover, a numerical simulation was conducted to evaluate the effects of self-weight and temperature stress on the secondary lining of the case tunnel. The results indicate that: the stress of the secondary lining concrete and steel bars is greatly affected by seasonal temperature changes. The compressive stress of the concrete and steel bars is significantly greater in summer than in winter, and the tensile stress is greater in winter than in summer. Furthermore, multiple measurement points have shown a phenomenon of transition between tensile and compressive stress states. The stress of concrete and steel bars fluctuates periodically with a sine function over time, with a fluctuation period of one year. The structural stress increases with the increase of summer temperature and decreases with the decrease of winter temperature. The fluctuation amplitude of stress in the inner side of the lining concrete and steel bars is greater than that on the outer side. Among them, the stress amplitudes of the inner and outer sides of the concrete are between 0.77–1.75 MPa and 0.44–1.07 MPa, respectively, and the stress amplitudes of the inner and outer steel bars are between 5–31 MPa and 7–13 MPa, respectively. The safety factors in summer are lower than those in winter. The minimum safety factors for secondary lining in summer and winter are 3.4 and 4.6, respectively, which can meet the safety requirements for service. The average axial forces of the secondary lining under the coupling effects of self-weight and temperature in winter and summer are 528 MPa and 563 MPa, respectively, which are significantly greater than the combined axial forces under their individual effects. The bending moment distribution of the secondary lining at the tunnel vault, inverted arch, wall spring and other positions under the coupling effect of self-weight and temperature is different from or even opposite to the bending moment superposition result under the two individual actions. The achieved results reveal that the influence of temperature stress on the service performance of the lining structure cannot be ignored, and the research results can provide useful reference for similar tunnels and related studies.

Keywords: tunnel engineering; super large-span tunnel; secondary lining; mechanical behavior; temperature stress

check for updates

Citation: Dong, F.; Luo, Y.; Chen, J.; Wang, C.; Liu, Y.; Xun, W. Mechanical Behavior of Secondary Lining in Super Large-Span Tunnels Considering Temperature Effects. *Symmetry* **2024**, *16*, 339. https://doi.org/10.3390/sym16030339

Academic Editors: Vasilis K. Oikonomou and Sergei D. Odintsov

Received: 18 January 2024
Revised: 24 February 2024
Accepted: 5 March 2024
Published: 12 March 2024

Copyright: © 2024 by the authors. Licensee MDPI, Basel, Switzerland. This article is an open access article distributed under the terms and conditions of the Creative Commons Attribution (CC BY) license (https://creativecommons.org/licenses/by/4.0/).

1. Introduction

With the rapid development of the social economy, traditional double-hole four-lane highway tunnels and double-hole six-lane highway tunnels can no longer meet the needs

of traffic growth and have even become bottlenecks that restrict social and economic development. Consequently, there has been a wave of building double-hole eight-lane highway tunnels in various regions [1–3]. The excavation span of a single-hole four-lane highway tunnel is generally greater than 18 m, and the tunnel structure is characterized by flat section and large span [4]. At present, the support structure of large-span tunnels adopts a composite lining structure of primary support and secondary lining, among which the secondary lining mostly uses formwork reinforced concrete [5]. Under the influence of periodic temperature changes, the secondary lining concrete of the tunnel will undergo thermal expansion (contraction) deformation, and the primary support and waterproof materials in contact with the secondary lining will constrain the deformation of the secondary lining, which will lead to temperature stress inside the secondary lining [6]. Concrete, as a type of cementitious material, has a tensile strength much lower than its compressive strength. Therefore, when subjected to tensile stress caused by a decrease in temperature, concrete is prone to cracking. Once cracks appear in the secondary lining of the tunnel, it will not only affect the stress of the lining structure, but also become a channel for water leakage [7]. Especially for single-hole four-lane highway tunnels, the section size and concrete volume of the secondary lining are larger than those of single-hole two-lane and three-lane tunnels. Under the action of temperature stress, cracks are more likely to occur in the secondary lining of a super large-span tunnel with four lanes in a single hole, and the harm of cracks is also more serious.

Due to the late start of single-hole four-lane highway tunnels, research in the field of tunnel engineering on large-span highway tunnels mainly focuses on single-hole three-lane highway tunnels and double-track railway tunnels [8–10], while there are limited studies on single-hole four-lane super large-span highway tunnels. Previous research on large-span highway tunnels has mainly focused on construction methods [11,12], support parameters [13–15], and stability control of surrounding rock [16–18] during construction. Nevertheless, there has been less attention paid to the stress properties of the secondary lining of large-span highway tunnels, and related research has mainly focused on load effects. Xu et al. [10] conducted model experiments and numerical simulations and found that due to the anisotropy of the rock mass and geo-stress field, the distribution of internal force and deformation of the secondary lining is uneven, and the axial forces and bending moments in the areas where the tangent line of the tunnel contour is parallel or perpendicular to the weak surface are more significant. Li et al. [19] conducted theoretical calculations and on-site monitoring and revealed that the measured internal force of the secondary lining was less than the values calculated by the load-structure model. The smaller the elastic resistance coefficient of the surrounding rock, the greater the bending moment on each section of the secondary lining, and the smaller the axial force and sectional safety factor. Fang et al. [20] conducted a load model test on the secondary lining of a large-span tunnel and found that under the combined action of surrounding rock pressure and external water pressure, the axial force of the secondary lining shows a conical distribution, and the axial force at the arch springs is greater than that at the invert and arch; the bending moment is distributed in a butterfly shape, with the arch springs bearing a positive bending moment and the inverted arch and tunnel vault bearing a negative bending moment; the arch springs has the maximum eccentricity, which is the most unfavorable position for the stress on the secondary lining of the tunnel. Wu et al. [21] studied the stress properties of the secondary lining of a three-lane highway tunnel through model experiments, and the results indicated that the internal force of the secondary lining increased slowly and then rapidly with the change of surrounding rock pressure, while the eccentricity gradually decreased. Moreover, the internal force at the arch springs, sidewall, and inverted arch was significant and reached failure first. Xu et al. [7] studied the deformation, internal force, and cracking properties of secondary lining under load−temperature coupling through physical model experiments, and the experimental results showed that the ultimate bearing capacity of the secondary lining decreased by 4% under repeated temperature cycling. The research on temperature stress in the field of tunnel engineering mainly focuses on tunnels

in cold regions [22]. Ling et al. [23] and Zhang et al. [24] studied the mechanical response of the lining of tunnels in cold regions under frost heave through theoretical analysis and numerical simulation. Li et al. [25,26] analyzed and discussed the mechanical behavior of the interaction between composite lining and surrounding rock in cold region tunnels under isotropic and anisotropic frost heave conditions and proposed the interaction behavior equation. Xu et al. [27] obtained the progressive degradation law of tunnel lining in cold regions through model experiments and numerical simulations, and the degradation of lining will promote crack development. Sutoh et al. [28,29] investigated the damage distribution characteristics and deterioration model of tunnel lining in cold regions to provide a basis for tunnel maintenance. However, previous studies have indicated that in non-cold regions, even in areas with distinct four seasons, the stress of the secondary lining of tunnels is affected by temperature stress [30]. Furthermore, previous research on the secondary lining of large-span highway tunnels has limited attention to temperature stress, especially in terms of the stress properties of the secondary lining of a single-hole four-lane super large-span highway tunnel under the coupling effect of load and temperature stress. As a result, the mechanical behavior and properties of the secondary lining under the coupling of load and temperature stress are not yet clear. Therefore, it is necessary to investigate the mechanical behavior and properties of the secondary lining of super large-span tunnels under the coupling effects of load and temperature stress.

The issue of the influence of temperature stress on general span tunnels is considered unimportant and often overlooked, but this influence cannot be ignored in super large-span tunnels. This paper presents a case study of the Letuan Tunnel, a super large-span highway tunnel with four lanes in a single hole, of the Binzhou-Laiwu expressway reconstruction and expansion project and focuses on the long-term mechanical response of secondary lining under load and temperature stress. Through detailed on-site stress monitoring, the variations of the concrete and steel bars of secondary lining with temperature were analyzed. Based on this, the effects of load and temperature on the service performance of the secondary lining were evaluated through numerical simulation, and finally the service performance of the secondary lining of super large-span tunnels under the combined effects of load and temperature was revealed. The present study could provide an important reference and basis for the research on the long-term stability and in-service durability of lining structures in super large-span tunnels.

2. Engineering Background and Test Scheme

2.1. Project Overview

Letuan Tunnel is located in Boshan District, Zibo City, Shandong Province. It is a typical double-hole eight-lane super large-span highway tunnel. Its maximum excavation span reaches 21.48 m, its maximum excavation height is 14.29 m, and its maximum excavation section area is 245.5 m^2. Its geographical location and tunnel portal are shown in Figure 1. The left line of the Letuan Tunnel is 2010 m long, the right line is 1995 m long, and the design speed is 100 km/h. It is a key control project of the Binzhou-Laiwu Expressway Renovation and Expansion Project. The Letuan Tunnel started construction in November 2016, and the left line of the tunnel was completed in mid-March 2018, and opened to traffic in September of the same year.

The tunnel site area belongs to the continental monsoon climate zone, and the local climate is significantly seasonal due to the influence of the monsoon. The winter climate is characterized by prevailing northerly winds, sparse rain and snow, and cold and dry conditions. The temperature rises quickly in spring, with less rain and more wind. The summer climate is characterized by high temperature and humidity, with concentrated precipitation. The precipitation in autumn sharply decreases, and the climate is cool and refreshing. The annual average temperature in the tunnel site area is between 12–13 °C. The highest temperature throughout a year is in July, with an average temperature of 25–26 °C, and the lowest temperature is in January, with an average temperature of −2.6–3.9 °C. There is a huge temperature gap between winter and summer.



Figure 1. Location and rock mass of the case tunnel.

The case tunnel was constructed using the drilling and blasting method. The surrounding rock of the entrance section is moderately weathered marl limestone. The rock mass was broken, the structural planes were developed, and the interlayer bonding was poor. The R_c ranges from 15.5 MPa to 34.2 MPa. According to the basic quality grading method of engineering rock mass (BQ method), the surrounding rock of the entrance section is classified as Grade-V. It should be noted that according to the BQ classification method, the surrounding rock can be divided into a total of 6 grades, with grades I to VI representing a gradual deterioration in the quality of the surrounding rock. This section was excavated using the upper-bench CD method, as illustrated in Figure 2. The cross-section and design support parameters of the Grade-V surrounding rock of the Letuan Tunnel are shown in Figure 3.



Figure 2. Upper-bench CD excavation method of Letuan Tunnel.

2.2. On Site Test Scheme

In order to analyze the stress properties of the secondary lining, a typical test cross-section was selected in the left line of Letuan Tunnel with Grade-V surrounding rock, and the section pile number is ZK105 + 952. The section was excavated on 10 August 2017, and the secondary lining concrete pouring was completed on 5 December 2017. Before the secondary lining construction, the surrounding rock was stabilized and the deformation rate was less than 0.06 mm/d. The secondary lining concrete stress and secondary lining reinforcement stress were monitored on site. The layout scheme of stress sensors is illustrated in Figure 4, and the on-site installation of the sensors is shown in Figure 5.

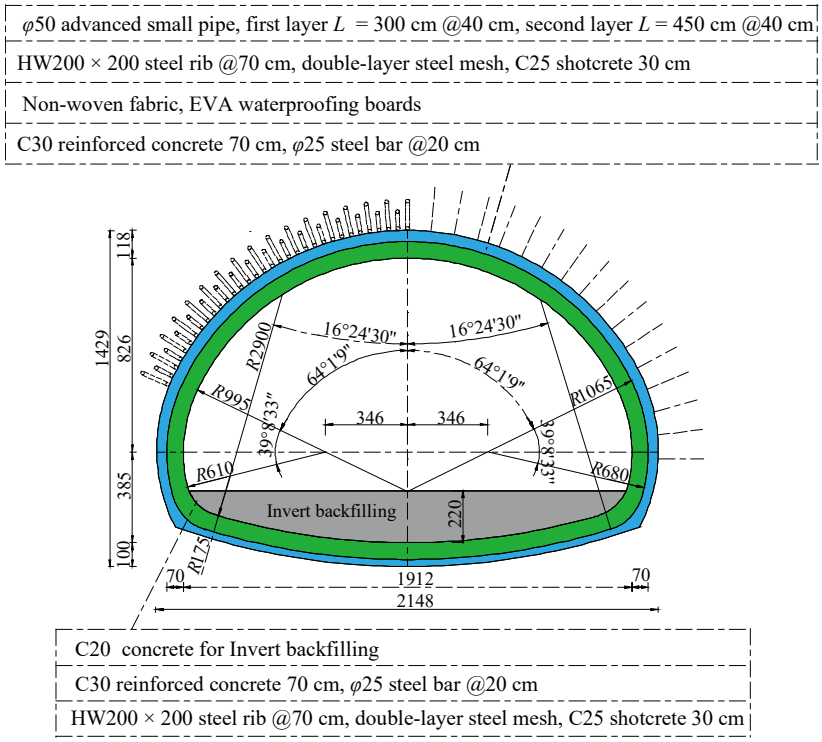


Figure 3. Cross-section and support parameters of Grade-V rock mass in Letuan Tunnel.

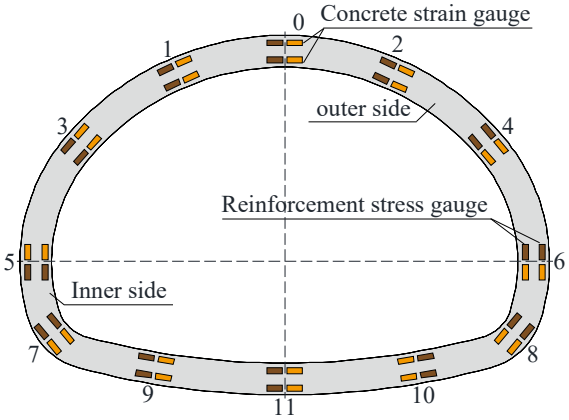


Figure 4. Layout diagram of secondary lining stress sensors.

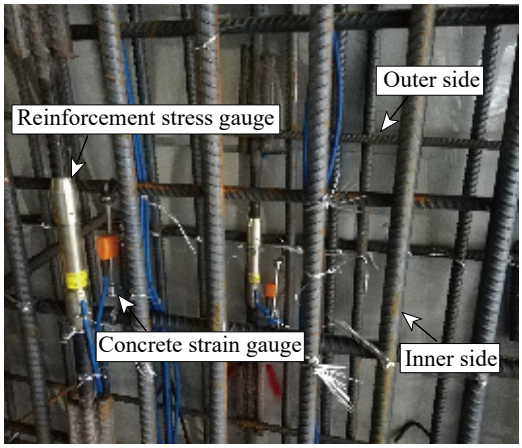


Figure 5. On-site installation of stress sensors.

Both the reinforcement stress gauge and the concrete strain gauge use vibrating wire sensors. The reinforcement stress gauge measures the axial force F_N of the steel bar, while the concrete strain gauge measures the strain of the concrete ε_h. According to the principle of coordinated deformation in material mechanics, the stress of steel bars σ_{gi} and concrete stress σ_{hi} can be calculated using Equations (1) and (2), respectively.

$$\sigma_{gi} = \frac{F_N}{A_g} \tag{1}$$

$$\sigma_{hi} = \varepsilon_h \cdot E_h \tag{2}$$

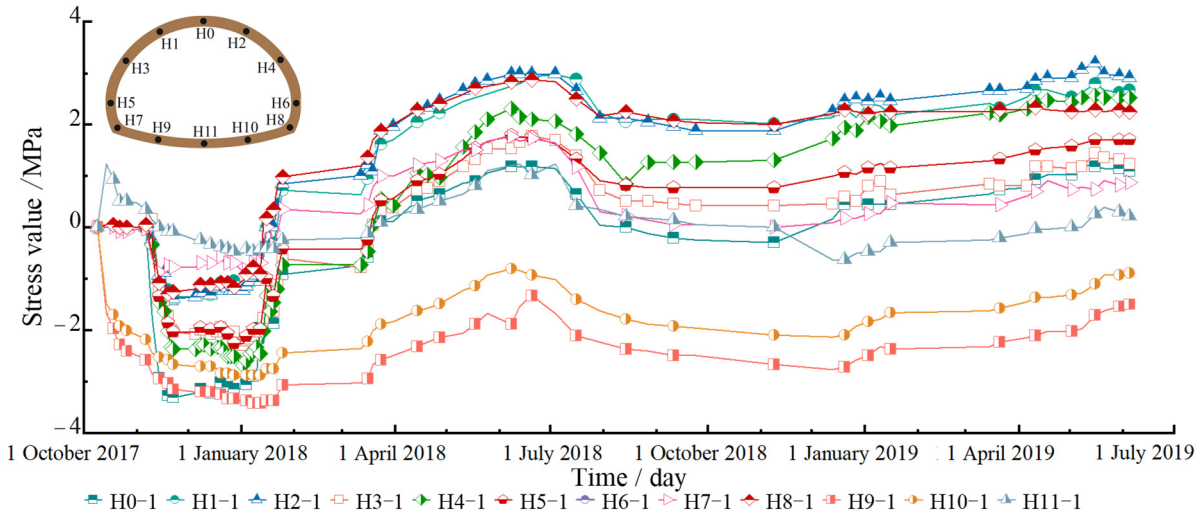
where, σ_{gi} represents the stress of the steel bars on the inner and outer sides of secondary lining. i = 1 or 2, with "1" indicating the outer side of secondary lining, and "2" indicating the inner side of secondary lining; F_N is the axial force of steel reinforcement; A_g is the cross-sectional area of steel reinforcement; σ_{hi} represents the stress of the concrete on the inner and outer sides of secondary lining; ε_h is the concrete strain; E_h is the elastic modulus of concrete.

3. Test Results and Analysis

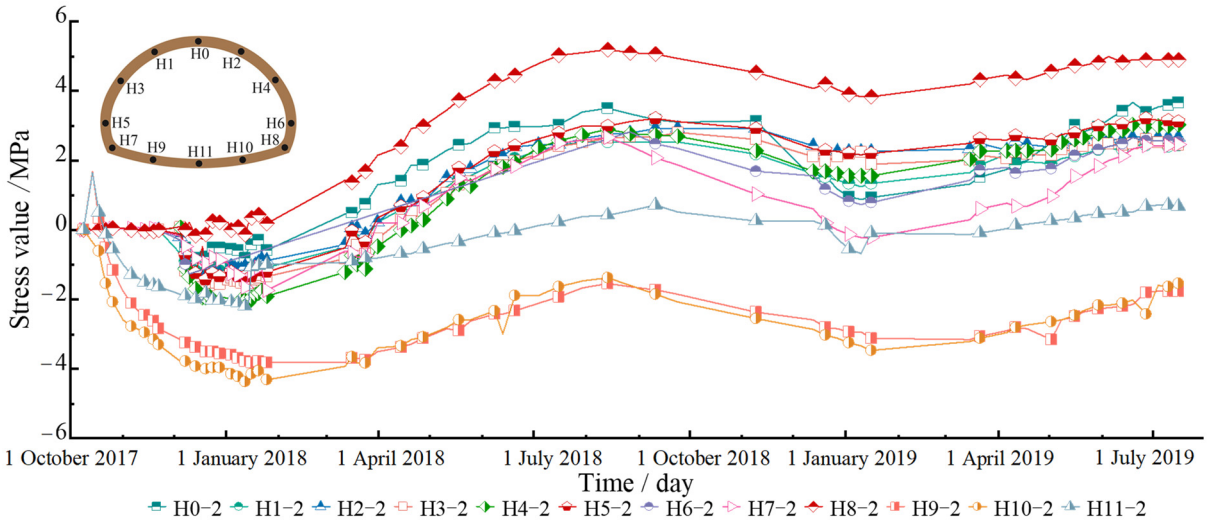
3.1. Concrete Stress of Secondary Lining

The stress monitoring results of the secondary lining concrete in section ZK105 + 952 of Letuan Tunnel are shown in Figure 6, with "+" indicating compression and "−" indicating tension.

It can be seen from Figure 6 that in the initial stage of secondary lining construction, the concrete is mainly subjected to tension and its stress increases rapidly. This is caused by the lower strength of the secondary lining concrete and the heat of hydration of the concrete. As the strength of concrete increases and the heat of hydration dissipates, the tensile stress value of the concrete decreases, and the tensile stress at most positions are converted to compressive stress. Furthermore, the secondary lining of section ZK105 + 952 was completed on 5 December 2017. By the time the tunnel was completed in March 2018, the hydration reaction inside the concrete had been completed, and the concrete strength met the design requirements. Therefore, after April 2018, with the natural circulation of air inside and outside the tunnel after it was completed, the impact of temperature changes on the stress of the secondary lining concrete gradually became apparent, and the concrete stress of the secondary lining changed periodically with time after April 2018. The concrete stress at each monitoring point reaches its maximum value in August (summer) and reaches its minimum value in January (winter). The primary reason is that the air temperature rises in summer and the secondary lining concrete expands in the circumferential direction, causing an increase in the structural internal force. In winter, the air temperature decreases, and the secondary lining concrete undergoes circumferential shrinkage, resulting in a decrease in the structural internal force. In addition, the concrete stress at the symmetrical position of the secondary lining cross-section exhibits asymmetric characteristics, which is a normal phenomenon and also in line with engineering practice. This difference is mainly caused by three factors. Firstly, the surrounding rock of the tunnel itself is anisotropic, and the attitude of the rock strata, such as a monoclinic structure, will generate asymmetric stress at symmetrical positions. Secondly, although the support parameter design of the secondary lining is symmetrical on both sides, there will always be slight differences in the actual construction process, such as pouring thickness and compaction density, resulting in different constraints on the symmetrical position of the cross-section. Thirdly, during on-site construction, excavation on both sides is often asynchronous and carried out in stages, resulting in asymmetric release of surrounding rock pressure.



(**a**)



(**b**)

Figure 6. Temporal curve of stress of secondary lining concrete in section ZK105 + 952. (**a**) Outer side of secondary lining. (**b**) Inner side of secondary lining.

According to the monitored stress results of secondary lining concrete, a statistical analysis was conducted on the extreme stress values and their differences of concrete at each monitoring point in winter and summer. The statistical results are listed in Table 1, and the stress distribution of the concrete in the cross-section of the secondary lining is shown in Figures 7 and 8. "Damaged" indicates that the embedded sensors are damaged during the secondary lining construction process of the tunnel and cannot measure data.

As shown in Table 1 and Figures 7 and 8, the stress distribution of the secondary lining concrete is uneven, and the overall compressive stress is dominant. Tensile stress mainly occurs in the inverted arch positions (No. 9, 10, and 11 monitoring points). In summer, the maximum compressive stress of the concrete in the arch appears at No. 0 monitoring point on the inner side of the secondary lining, reaching 3.31 MPa. In winter, the maximum compressive stress of the concrete in the arch appears at the No. 2 monitoring point on the inner side of the secondary lining, reaching 2.24 MPa. The compressive stress of the secondary lining concrete in summer and winter is less than its ultimate compressive strength of 22.5 MPa, but the tensile stress of the concrete in the inverted arch is close to

or even exceeds its ultimate strength. Especially in winter, when the concrete shrinks due to cold conditions, there are some positions in the inverted arch where the tensile stress exceeds the ultimate tensile strength, posing a risk of cracking.

Table 1. Statistics of stress difference in concrete between winter and summer (Unit: MPa).

Items		Positions											
		0	**1**	**2**	**3**	**4**	**5**	**6**	**7**	**8**	**9**	**10**	**11**
Outer side	Summer	1.04	2.84	2.85	1.62	1.51	1.62	/	1.58	2.72	−1.47	−0.98	1.10
	Winter	−0.27	2.04	1.89	0.49	0.83	0.76	/	0.03	2.07	−2.65	−2.07	−0.61
	Difference	1.31	0.8	0.96	1.13	0.68	0.86	/	1.55	0.65	1.18	1.09	1.71
Inner side	Summer	3.31	2.41	2.76	2.67	2.81	3.05	/	2.48	5.00	−1.72	−1.55	0.57
	Winter	0.86	1.26	2.24	1.92	1.55	2.19	/	−0.21	3.86	−3.09	−3.45	−0.68
	Difference	2.45	1.15	0.52	0.75	1.26	0.86	/	2.69	1.14	1.37	1.90	1.25

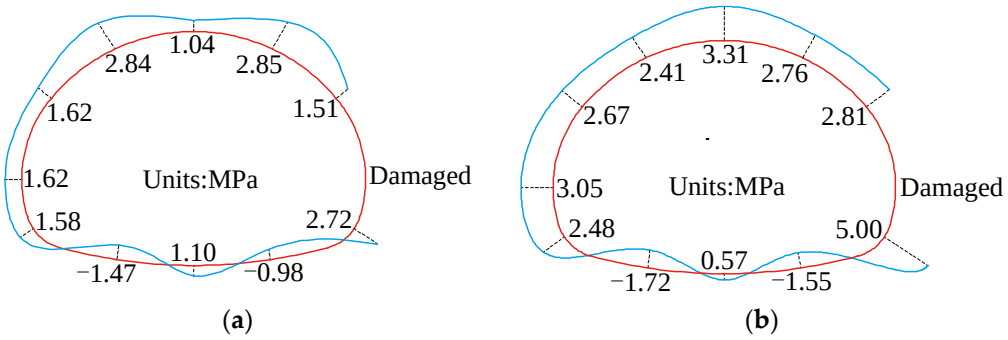


Figure 7. Stress distribution of secondary lining concrete on section ZK105 + 952 in summer. (**a**) Outer side. (**b**) Inner side.

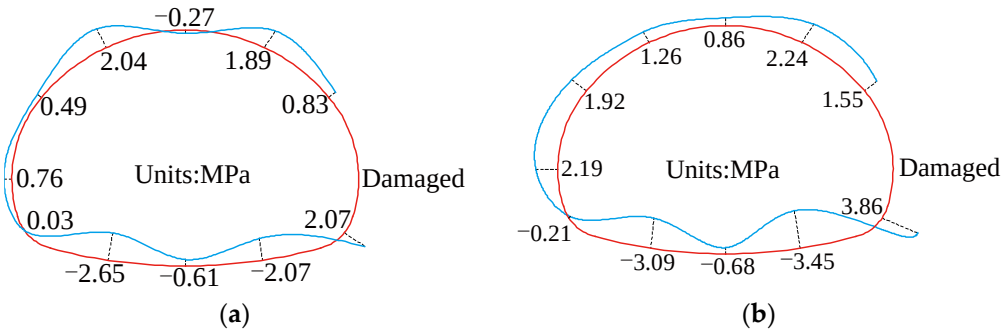


Figure 8. Stress distribution of secondary lining concrete on section ZK105 + 952 in winter. (**a**) Outer side. (**b**) Inner side.

In addition, the maximum difference in concrete stress on the outer side of the secondary lining at the upper arch and sidewalls between summer and winter reaches 1.31 MPa, with an average value of 0.96 MPa. The maximum difference in concrete stress on the inner side of the secondary lining at the upper arch and sidewalls between summer and winter reaches 2.45 MPa, with an average value of 1.17 MPa. The maximum difference in concrete stress on the outer side of the secondary lining at the inverted arch between summer and winter reaches 1.55 MPa, with an average value of 1.24 MPa. The maximum difference in concrete stress on the inner side of the secondary lining at the inverted arch between summer and winter reaches 2.69 MPa, with an average value of 1.67 MPa. It is evident that temperature changes have a significantly greater impact on the concrete stress on the inner side of the secondary lining than that on the outer side. Moreover, the stress variation of the inverted arch under the influence of temperature stress is more significant than that of the upper arch and sidewalls, which seems to be inconsistent with general

understanding. Analysis suggests that this is mainly caused by the following two reasons. Firstly, although the backfilling of the inverted arch and the pavement structure may delay the transfer of air temperature to the secondary lining, due to the good thermal conductivity of concrete itself and its larger specific heat capacity than air, the extreme temperature conducted by the covering layer has a longer duration of impact on the inverted arch. Secondly, the secondary lining is a circular structure, and the influence of temperature on the stress of the upper arch and sidewalls of the secondary lining will be transmitted downwards and accumulate at the inverted arch, resulting in more significant changes in the stress of the inverted arch.

Concrete is a material with good thermal conductivity, and the temperature change of the airflow inside the tunnel directly affects the structural temperature of the secondary lining. During the long-term operation of the tunnel, the temperature gap between the air temperature and the structure temperature is small. As a narrow cylindrical structure located underground, the secondary lining is constrained by the surrounding rock and primary support in both radial and axial directions. When the temperature of the air inside the tunnel increases, the thermal expansion deformation of the secondary lining concrete material is restricted, resulting in an increase in the contact force between particles inside the secondary lining concrete. This is manifested as an increase in compressive stress or a decrease in tensile stress along the tunnel circumferential direction. On the contrary, when the temperature inside the tunnel decreases, the secondary lining concrete shrinks, resulting in an increase in tensile stress or a decrease in compressive stress along the tunnel circumferential direction.

3.2. Reinforcement Stress of Secondary Lining

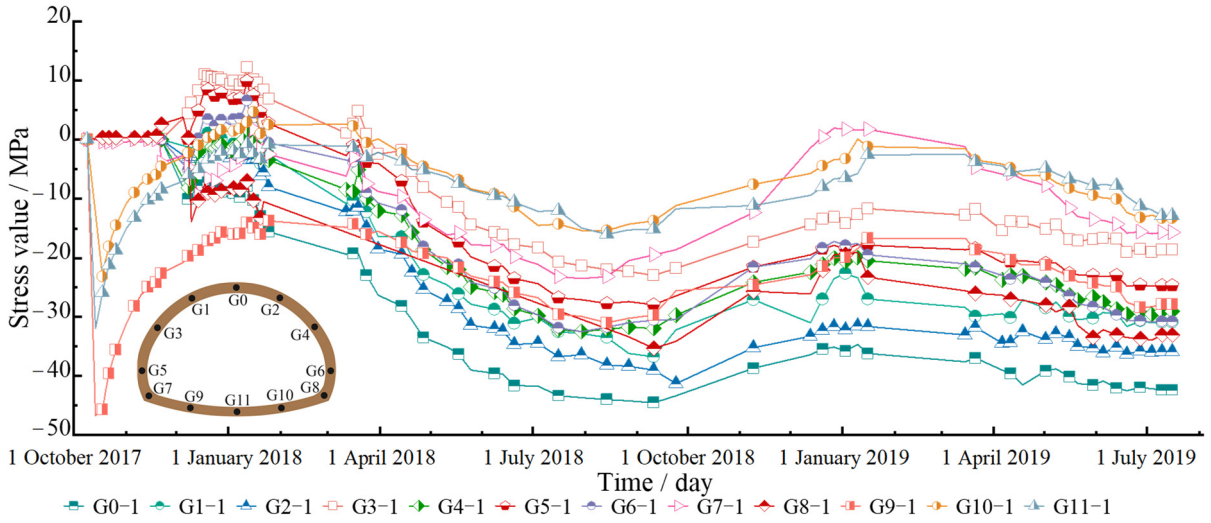
The stress monitoring results of the secondary lining reinforcement in the section ZK105 + 952 of the Letuan Tunnel are shown in Figure 9.

As shown in Figure 9, the temperature has a great impact on the reinforcement stress of the secondary lining. There is a clear periodic variation in the stress temporal curves of the reinforcement with the periodic change of air temperature. In the early stage after the secondary lining construction, due to the hydration reaction of the concrete, the compressive stress of the steel bars increases sharply in a short period of time. After about 7 days, the stress of the steel bars gradually decreases with the improvement of the bearing capacity of the secondary lining and the dissipation of hydration heat. Afterwards, the stress of the steel bars entered a slow growth stage, and the overall compressive stress of the inner and outer steel bars was dominant. After April 2018, the stress of the steel bars in the secondary lining began to show significant periodic changes with temperature, for the same reason as the stress changes in the secondary lining concrete.

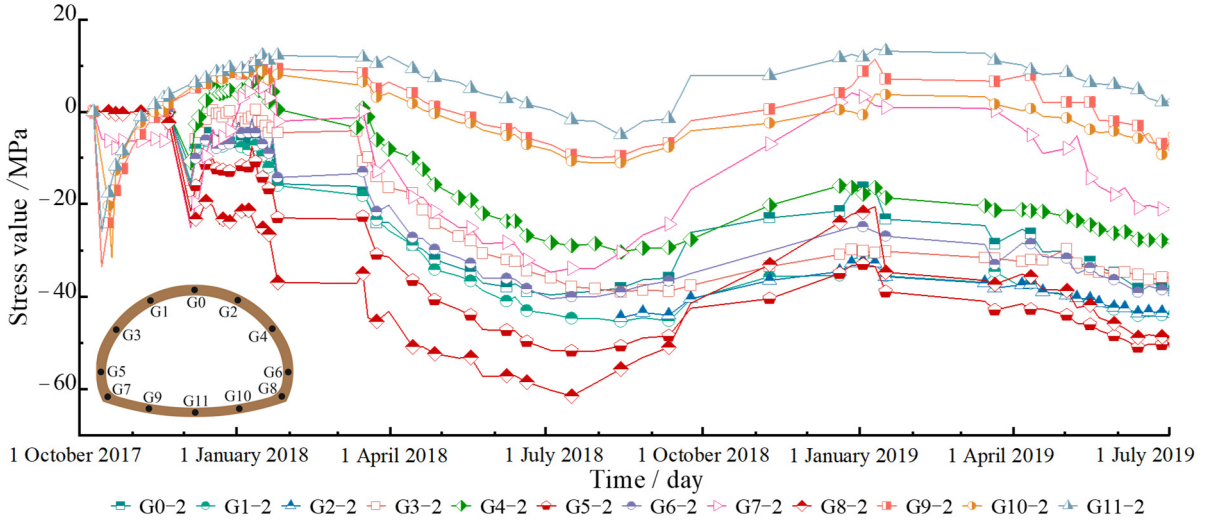
A statistical analysis was conducted on the extreme stress and their differences in the steel bars at each monitoring point in winter and summer. The statistical results are listed in Table 2, and the stress distribution of the steel bars of the secondary lining is displayed as Figures 10 and 11.

Table 2. Statistics of stress difference in steel bars between winter and summer (Unit: MPa).

Items		Positions											
		0	**1**	**2**	**3**	**4**	**5**	**6**	**7**	**8**	**9**	**10**	**11**
Outer side	Summer	−45	−37	−39	−23	−32	−28	−33	−24	−38	−31	−14	−16
	Winter	−35	−23	−31	−14	−20	−18	−17	2	−19	−18	0	−6
	Difference	−10	−14	−8	−9	−12	−10	−16	−26	−19	−13	−14	−10
Inner side	Summer	−40	−45	−45	−39	−30	−52	−40	−35	−62	−10	−5	−11
	Winter	−17	−31	−32	−30	−16	−33	−29	5	−21	11	4	14
	Difference	−23	−14	−13	−9	−14	−19	−11	−40	−41	−21	−9	−25

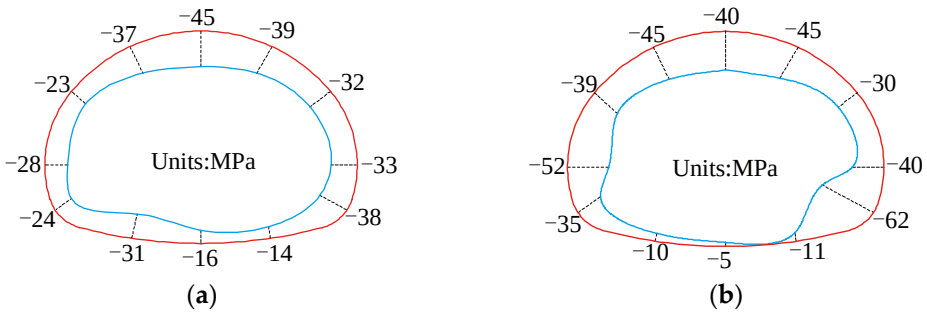


(**a**)



(**b**)

Figure 9. Temporal curve of stress of steel bars in the secondary lining of section ZK105 + 952. (**a**) Outer side. (**b**) Inner side.



(**a**) (**b**)

Figure 10. Stress distribution of steel bars in the secondary lining of section ZK105 + 952 in summer. (**a**) Outer side. (**b**) Inner side.

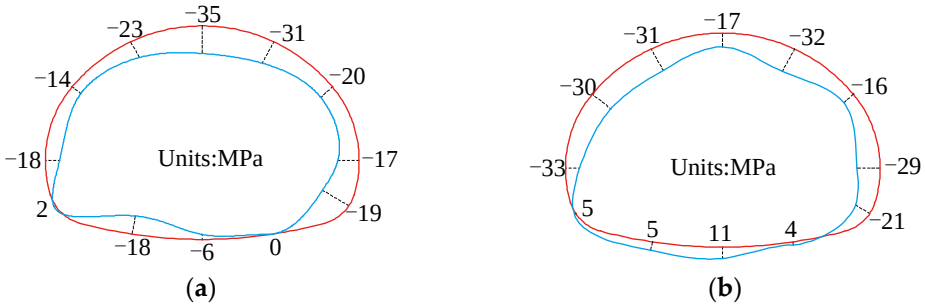


Figure 11. Stress distribution of steel bars in the secondary lining of section ZK105 + 952 in winter. (**a**) Outer side. (**b**) Inner side.

It can be seen from Table 2 and Figures 10 and 11 that the steel bars of the secondary lining are mainly subjected to compressive stress, and the stress distribution is uneven. In summer, the maximum compressive stress of the steel bars on the outer side of the secondary lining reaches 45 MPa, which occurred at the tunnel vault (No. 0 monitoring point). The maximum compressive stress of the steel bars on the inner side of the secondary lining reaches 62 MPa, which occurred at the right wall corner (No. 8 monitoring point). The stress value of steel bars is much less than its yield strength of 400 MPa. In winter, the maximum compressive stress of the steel bars on the outer side of the secondary lining is 35 MPa, which is located at the tunnel vault (No. 0 monitoring point). The maximum compressive stress of the steel bars on the inner side of the secondary lining is 33 MPa, which is located at the left arch springs (No. 5 monitoring point). The reinforcement stress of the secondary lining at the same position is significantly different between winter and summer.

Monitored results indicate that temperature has a great influence on the reinforcement stress of the secondary lining and cannot be ignored. The stress difference range of the outer side steel bars is 8–26 MPa, and the maximum difference occurs at the left wall corner (No. 7 monitoring point). The stress difference range of the inner side steel bars is 9–41 MPa, and the maximum difference occurs at the right wall corner (No. 8 monitoring point). Meanwhile, the average difference in stress of the steel bars on the outer side of the secondary lining at the upper arch and sidewalls between summer and winter reaches 11.3 MPa, and the average difference in stress of the steel bars on the outer side of the secondary lining at the inverted arch between summer and winter reaches 16.4 MPa. The average difference in stress of the steel bars on the inner side of the secondary lining at the upper arch and sidewalls between summer and winter reaches 20.6 MPa, and the average difference in stress of the steel bars on the inner side of the secondary lining at the inverted arch between summer and winter reaches 27.2 MPa. Consistent with the stress variation law of concrete, the stress variation of steel bars under the influence of temperature stress also shows the characteristics of inner side greater than outer side, and inverted arch greater than arch wall.

3.3. Fitting Analysis of Secondary Lining Stress

The left line of Letuan Tunnel was completed in March 2018. To accurately analyze the stress variation of secondary lining over time, measured data after 31 March were selected for fitting analysis of the time−stress relationship. Taking the inner side of the concrete and the outer side of the steel bar as an example, the fitting results of typical monitoring points are listed in Tables 3 and 4.

Table 3. Stress fitting results of concrete (inner side).

Monitoring Point	Fitting Mathematical Model	Correlation Coefficient
No. 0	$\sigma_{H0} = 1.34\sin(2\pi\frac{t-32.98}{365}) + 2.28$	0.95
No. 7	$\sigma_{H7} = 1.37\sin(2\pi\frac{t-35.72}{365}) + 1.15$	0.94
No. 10	$\sigma_{H10} = 0.94\sin(2\pi\frac{t-45.53}{365}) - 2.52$	0.95

Table 4. Stress fitting results of steel bar (outer side).

Monitoring Point	Fitting Mathematical Model	Correlation Coefficient
No. 7	$\sigma_{G7} = -11.83\sin(2\pi\frac{t-30.82}{365}) - 10.03$	0.96
No. 10	$\sigma_{G10} = -7.06\sin(2\pi\frac{t-46.6}{365}) - 7.59$	0.94
No. 11	$\sigma_{G11} = -6.15\sin(2\pi\frac{t-67.18}{365}) - 8.96$	0.95

It can be seen from the fitting results in Tables 3 and 4 that the concrete stress (σ_H) and the steel reinforcement stress (σ_G) fluctuate periodically with a sinusoidal function over time (t), and the fluctuation period is 365 days (one year). It is obvious that this is a structural stress change that varies with seasonal temperature changes in the tunnel site area.

The stress-time fitting curves of the concrete and steel bars at typical monitoring points of secondary lining are shown in Figures 12 and 13.

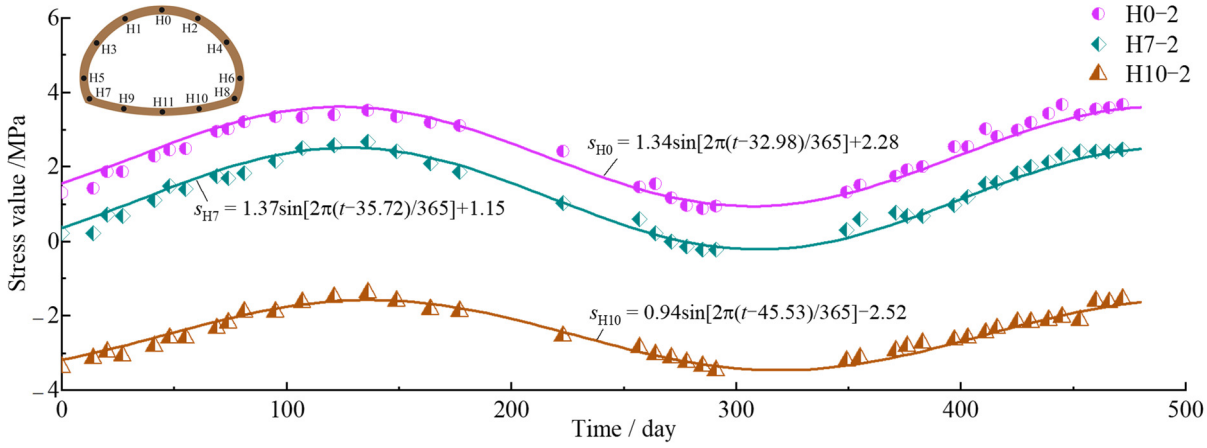


Figure 12. Stress-time fitting curves of concrete.

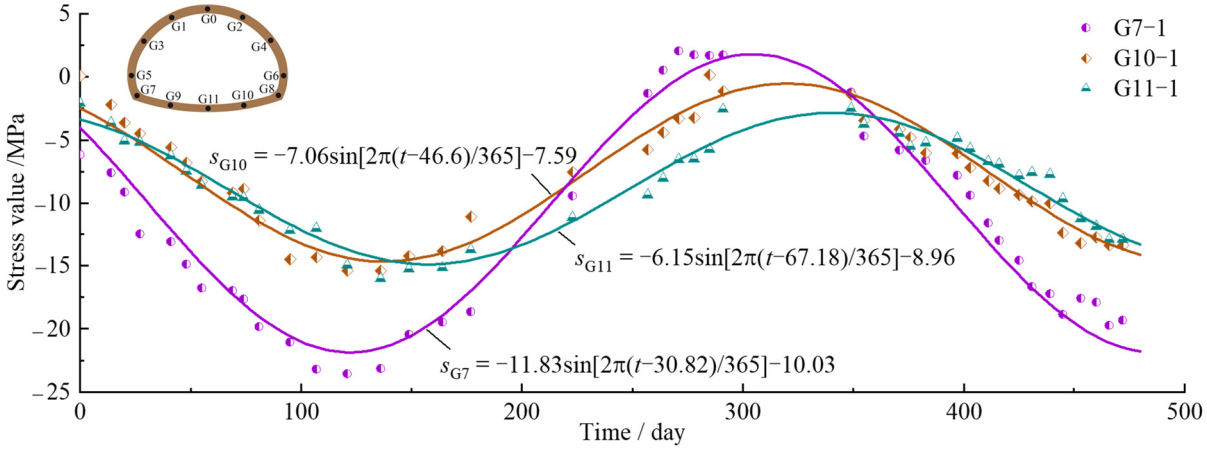


Figure 13. Stress-time fitting curves of steel bars.

From Figures 12 and 13, it can be seen that both concrete stress and steel stress fluctuate periodically with time, and the fitting relationship conforms to the sine function. The fitting effect is good, and the correlation coefficients are not less than 0.94. The distribution law of concrete is more uniform and consistent, which is related to the uniform distribution and vibration of concrete. The overall law of steel stress is the same, but there are still slight differences. The main reason is that the restraint conditions of steel bar binding and welding are different, resulting in different stress changes. Combining the monitored stress data after 31 March 2018, it can be seen that the maximum amplitude of the stress on the outer side of the concrete reaches 2.13 MPa, and the minimum amplitude is 0.88 MPa. The maximum amplitude of the stress on the inner side of the concrete peaks 3.50 MPa, and the minimum amplitude is 1.53 MPa. The maximum amplitude of the stress on the outer side of the steel bars is 25.6 MPa, and the minimum amplitude is 13.9 MPa. The maximum amplitude of the stress on the inner side of the steel bars reaches 61.6 MPa, and the minimum amplitude is 9.3 MPa. The stress changes with time of the concrete and steel bars on the inner side of the secondary lining are greater than those on the outer side. The main reason is that the inner side of the secondary lining is closer to the tunnel clear surface and more sensitive to temperature changes than the outer side.

3.4. Secondary Lining Safety

The secondary lining contains two layers of steel bars. The structural circumferential stress can be simplified as a calculation model for eccentrically compressed rectangular section components. The internal force calculation model of the secondary lining section is shown in Figure 14 [4].

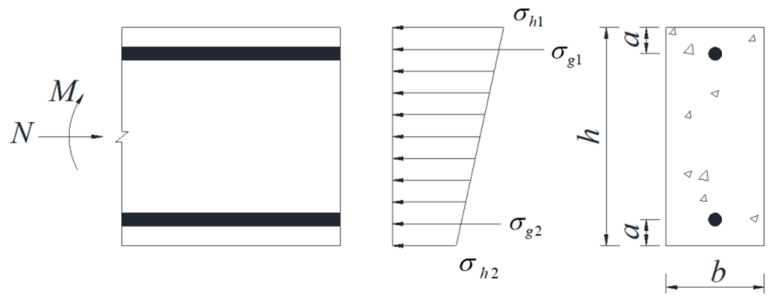


Figure 14. Calculation model for the section internal force of secondary lining.

According to the static equilibrium conditions, it can be shown that:

$$N = \frac{1}{2}(\sigma_{h1} + \sigma_{h2})(b \times h) + (\sigma_{g1} + \sigma_{g2})A_s \tag{3}$$

$$M = (\sigma_{g1} - \sigma_{g2})A_g(\frac{h}{2} - a) + \frac{1}{8}h(\sigma_{c1} - \sigma_{c2})(b \times h) \tag{4}$$

where, M and N are the sectional bending moment and axial force of secondary lining; M_g is the bending moment borne by steel reinforcement; a is the thickness of the steel reinforcement cover layer, taken as 6 cm according to the design of the case tunnel; h is the thickness of secondary lining; b is the length of the calculation unit, taking b = 10 + 2.5 + 10 = 22.5 cm.

The secondary lining of the tunnel mainly manifests as a compressed state, and the structural safety factor can be calculated using the strength verification method for eccentrically compressed reinforced concrete rectangular section members. The calculation diagram of the safety factor of the secondary lining section is shown in Figure 15, and the specific calculation method is shown in Equations (5)–(9).

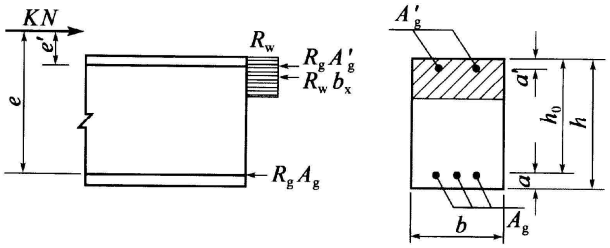


Figure 15. Calculation diagram of eccentric compressive strength of reinforced concrete rectangular cross-section.

The formula for calculating the comprehensive safety factor is:

$$KN \leq R_a bx + R'_g A'_g - \sigma_g A_g \tag{5}$$

The calculation formula for neutral axis position is:

$$R_a bx(e - h_0 + \frac{x}{2}) = \sigma_g A_g e + R'_g A'_g e' \tag{6}$$

when $x \leq 0.55h_0$, the secondary lining belongs to a large eccentric compression component, and σ_g in Equations (5) and (6) should be taken as R_g. When $x > 0.55h_0$, the secondary lining belongs to a small eccentric compression component, and σ_g can be calculated according to Equation (7).

$$\sigma_g = 0.003E_g(\frac{0.9h_0}{x} - 1) \tag{7}$$

For large eccentrically compressed components, when considering compressive steel bars in the calculation, the height of the concrete compression zone must meet $x \geq 2a'_g$. If it is not met, the strength of the normal section of the component needs to be calculated according to Equation (8).

$$KNe' \leq R_g A_g(h_0 - a'_g) \tag{8}$$

For small eccentrically compressed components, if the axial force acts between the resultant force point of the steel reinforcement A_g and the resultant force point of the steel reinforcement A'_g, the strength of the normal section of the component also needs to comply with Equation (9).

$$KNe' \leq 0.5R_a bh'^2_0 + R'_g A_g'(h'_0 - a_g) \tag{9}$$

where, K is the safety factor of the secondary lining, R_a is the standard compressive strength of concrete, R_g is the standard tensile strength of steel reinforcement, x is the height of the compression zone, h_0 is the effective height of the cross-section, h'_0 is the distance from the resultant force point of the compressed steel bar to the edge of the section near the tensioned steel bar, a'_g is the distance from the resultant force point of the compressed steel bar to the edge of the section, a_g is the distance from the resultant point of the tensile steel reinforcement to the edge of the section, e' is the distance from the resultant point of axial force to the resultant points of steel reinforcement in the tension and compression zones.

According to the stress peaks of secondary lining measured in winter and summer, the safety factor at each monitoring point of the secondary lining was calculated using the method mentioned above. The calculation results are displayed in Figure 16.

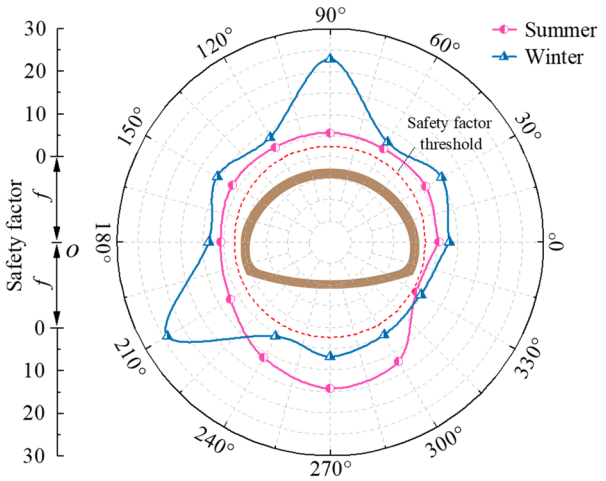


Figure 16. Safety factor distribution on cross-section.

As shown in Figure 16, the safety factors of the secondary lining in winter and summer are greater than the critical value of 2.4. In winter, the safety factors of the secondary lining vary greatly, with the maximum value appearing at the left wall corner (210°), followed by the arch crown (90°), and the minimum value appearing at the right wall corner (330°). In summer, the safety factor of the secondary lining at each measuring point in the tunnel arch is relatively close, with a value of around 5.0. The safety factors at the inverted arch are greater than those at the tunnel arch. Overall, the safety factor of the secondary lining follows the pattern of "winter is greater than summer for the tunnel arch, and summer is greater than winter for the inverted arch". The minimum safety factors for the secondary lining in winter and summer are 4.6 and 3.4, respectively, and the safety factor in summer is 26% lower than that in winter.

4. Numerical Simulation and Analysis

Before the secondary lining construction of the sections ZK105 + 942–ZK105 + 957 of the Letuan Tunnel, the surrounding rock pressure of the tunnel and the internal force of the primary support had stabilized with no more growth [5]. Therefore, this suggests that the secondary lining is only used as a safety reserve layer for the tunnel, and the load transferred from the surrounding rock and primary support is not considered when establishing a tunnel model. When analyzing the stress properties of the secondary lining of a single-hole four-lane super large-span highway tunnel, only two factors, temperature stress and gravity load, were considered. Three working conditions, namely, gravity load, temperature stress, and gravity load + temperature stress are simulated.

4.1. Establishment of Numerical Models

4.1.1. Numerical Calculation Process

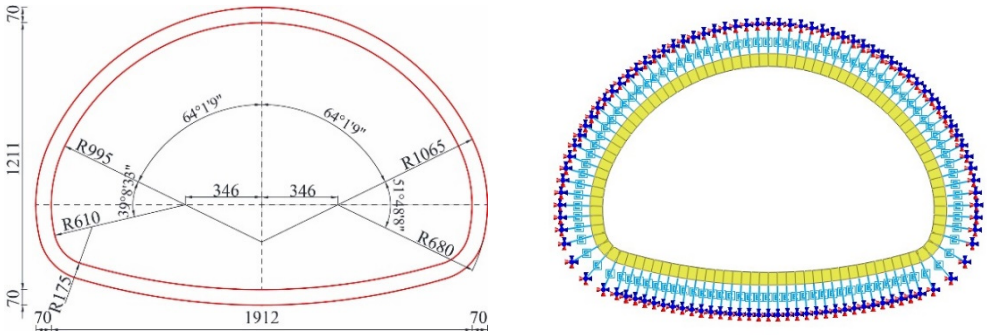
MIDAS-GTS NX 2021 is a universal finite element analysis software developed for the field of geotechnical tunnels, with powerful pre-processing and solving functions. This software is suitable for accurate modeling, structural calculation, and thermodynamic analysis of various practical engineering projects such as tunnels, slopes, foundation pits, etc. A load-structure method model was established to numerically simulate the stress state of the secondary lining using MIDAS-GTS NX 2021 software. To simplify calculations, beam elements are used to simulate secondary lining. The interaction between the secondary lining and the primary support is simulated using curved springs and the curved springs are set to a compressed state. The elastic resistance coefficient of curved springs is determined according to the Specifications for Design of Highway Tunnels (JTG 3370.1-2018) [31].

4.1.2. Numerical Model Parameters

The thicker the secondary lining, the larger the volume of the secondary lining, the slower the heat exchange, and the more significant the temperature stress caused by thermal expansion and contraction under the constraint of the surrounding primary support [32]. Therefore, the secondary lining of the Grade-V surrounding rock section of the Letuan Tunnel is selected for numerical calculation and analysis. Based on the actual support parameters of the secondary lining on site, and referring to the relevant provisions of the Specifications for Design of Highway Tunnels (JTG 3370.1-2018) [31] and previous research results of similar projects 7,10, appropriate physical and thermodynamic parameters of the secondary lining are selected, as listed in Table 5. The calculation model is set according to the actual size of the secondary lining, with a grid size controlled at 1 m. The cross-section and calculation model of the secondary lining of the Letuan Tunnel are illustrated in Figure 17.

Table 5. Physical and thermodynamic parameters of secondary lining.

Rock Grade	Materials	Thickness/cm	Elastic Modulus/GPa	Poisson's Ratio μ	Gravity Density/KN·m^{-3}	Linear Expansion Coefficient/°C^{-1}
V	C30 reinforced concrete	70	32.4	0.20	23	1.05×10^{-5}



(**a**) (**b**)

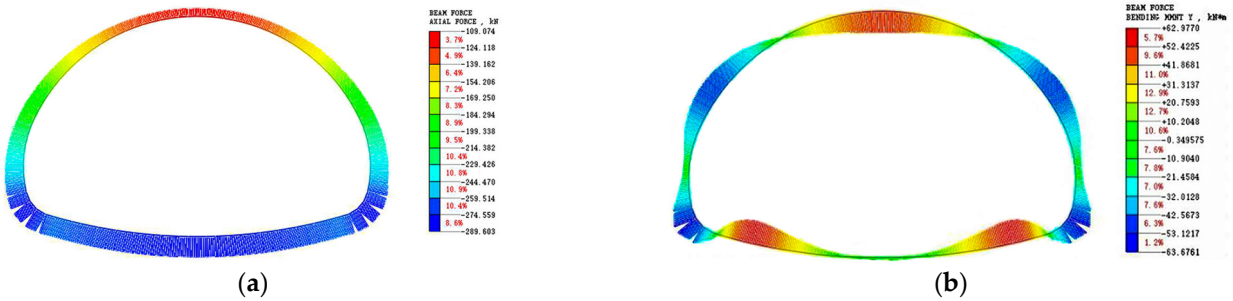
Figure 17. Numerical model of secondary lining of Letuan Tunnel. (**a**) Cross-section of secondary lining. (**b**) Numerical model.

Considering that the average temperature in April in the tunnel site area is the middle value of the average temperature in a year, the measured average temperature in April (15 °C) at the section ZK105 + 952 of the Letuan Tunnel is taken as the initial temperature, the lowest temperature throughout the year (−9 °C) is taken as the winter calculated temperature, and the highest temperature throughout the year (34 °C) is taken as the summer calculated temperature for simulation.

4.2. Simulation Results and Analysis

4.2.1. Mechanical Behavior of Secondary Lining under Gravity Load

The structural axial force and bending moment of the secondary lining under its own weight are shown in Figure 18. According to the numerical calculation results, the axial force and bending moment values of key sections (see Figure 19) such as the tunnel vault, arch waist, arch springs, and inverted arch were extracted, and the safety factors of each section of the secondary lining were calculated based on this. The results are listed in Table 6.



(**a**) (**b**)

Figure 18. Internal force of secondary lining under self-weight. (**a**) Axial force. (**b**) Bending moment.

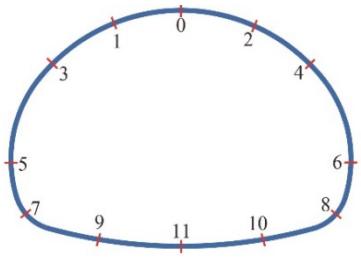


Figure 19. Typical positions and numbering of cross-section.

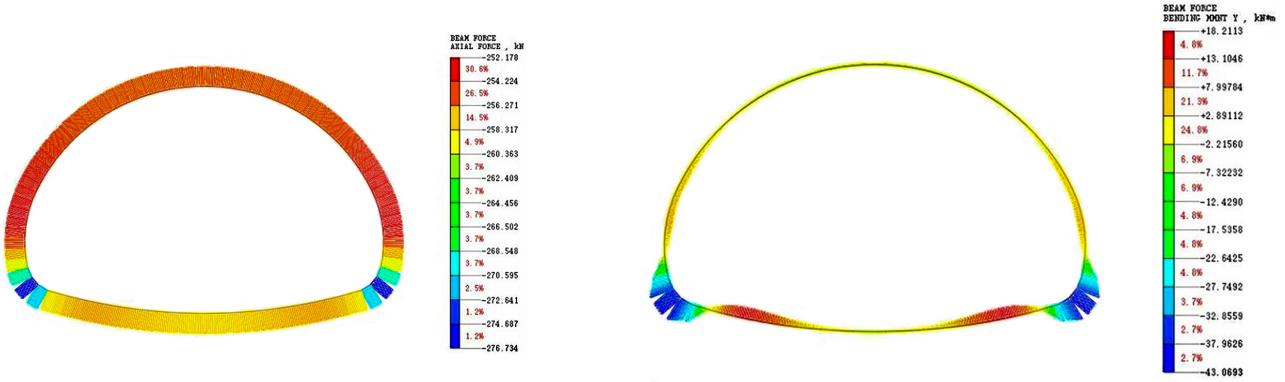
Table 6. Simulation results of internal forces in secondary lining under gravity load.

Positions	0	1	2	3	4	5	6	7	8	9	10	11
Axial force (kN)	109.3	122.1	122.1	182.5	182.5	245.3	245.3	277.3	277.3	284.7	284.7	288.7
Bending moment (kN·m)	57.0	28.0	28.0	−52.7	−52.7	−14.2	−14.2	−63.7	−63.7	19.0	19.0	4.0
Safety factor	10.1	13.2	13.2	8.1	8.1	9.0	9.0	5.8	5.8	7.6	7.6	8.4

According to Figure 18 and Table 6, it can be seen that because the gravity load is completely symmetrically applied to the secondary lining, the axial force and bending moment obtained are also symmetrical on both sides. When only bearing its self-weight, the secondary lining is in a compressed state as a whole, with the minimum axial force appearing at the tunnel vault and the maximum axial force appearing at the inverted arch. The maximum axial reaches 288.7 KN; the tunnel vault and inverted arch are subjected to positive bending moments, while the bending moments at the arch waist, arch springs, and wall springs are negative. The maximum positive bending moment reaches 57.0 kN·m (No. 0 monitoring point), and the maximum negative bending moment is −52.7 kN·m (No. 3 and No. 4 monitoring points). The safety factor of the secondary lining ranges from 5.8 to 13.2, with the minimum value appearing at No. 7 and No. 8 monitoring points, indicating that the left and right wall feet are the most unfavorable positions for the structural stress. However, the safety factor of the lining structure meets the threshold of the critical threshold (2.0) and still meets the operational safety requirements. Compared with the safety factors determined by the measured stress, it can be seen that the minimum safety factor of both occurs at the sidewall springs. However, the minimum safety factor determined by on-site measurement is smaller than that determined by simulation (only bearing gravity load), which is about 59% of the latter.

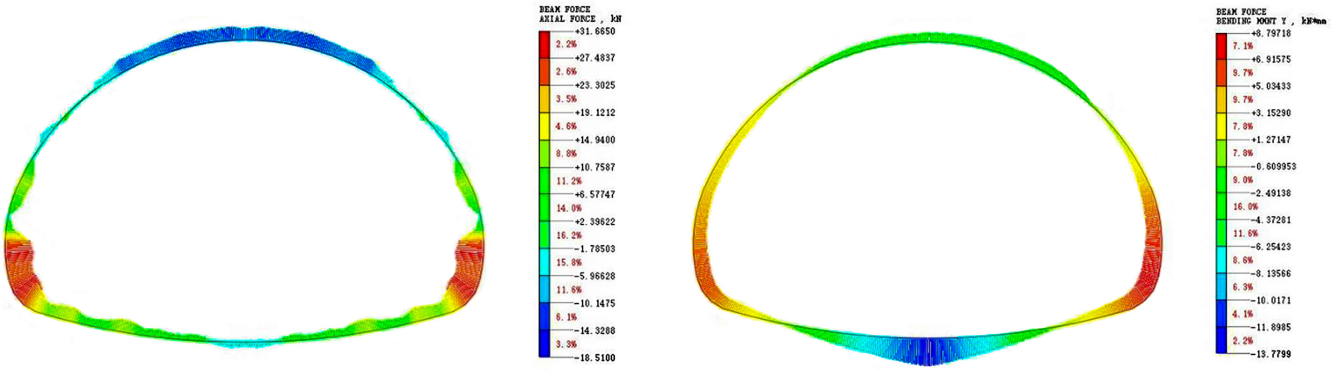
4.2.2. Mechanical Behavior of Secondary Lining under Temperature Stress

Only temperature loads were applied to the secondary lining model, and the axial forces and bending moments obtained in summer and winter are shown in Figures 20 and 21. The statistical values of axial forces and bending moments on key sections are listed in Table 7.



(**a**) (**b**)

Figure 20. Internal force of secondary lining in summer. (**a**) Axial force. (**b**) Bending moment.



(**a**) (**b**)

Figure 21. Internal force of secondary lining in winter. (**a**) Axial force. (**b**) Bending moment.

Table 7. Simulation results of internal forces in secondary lining under temperature stress.

Seasons	Positions	0	1	2	3	4	5	6	7	8	9	10	11
Summer	Axial force (kN)	254.0	254.0	254.0	253.5	253.5	252.1	252.1	276.7	276.7	256.0	256.0	256.7
	Bending moment (kN·m)	−1.5	−1.7	−1.7	3.0	3.0	8.7	8.7	41.2	41.2	15.6	15.6	−1.5
	Safety factor	9.7	9.7	9.7	9.6	9.6	9.2	9.2	6.7	6.7	8.5	8.5	9.6
Winter	Axial force (kN)	11.1	15.0	15.0	2.8	2.8	−31.5	−31.5	−31.7	−31.7	−12.9	−12.9	2.7
	Bending moment (kN·m)	38.1	26.6	26.6	−38.4	−38.4	−62.1	−62.1	−70.0	−70.0	67.6	67.6	137.8
	Safety factor	24.1	31.4	31.4	26.0	26.0	13.7	13.7	12.4	12.4	14.1	14.1	7.4

According to Table 7 and Figures 20 and 21, it can be seen that because temperature stress uniformly acts on the entire lining structure, the internal forces of the secondary lining are symmetrically and uniformly distributed on both sides, whether in summer or winter.

When the temperature rises in summer, under the action of temperature stress, the secondary lining is in a fully compressed state, with the minimum axial force value occurring at the arch, followed by the inverted arch, and the maximum axial force appears at the feet of the sidewalls, reaching 276.7 kN; the secondary lining arch waist and wall springs bear positive bending moments, while the tunnel vault and inverted arch bear negative bending moments. The maximum positive bending moment occurs at No. 7 and No. 8 monitoring points, reaching 41.2 kN·m, and the maximum negative bending moment occurs at No. 1 and No. 2 monitoring points, reaching −1.7 kN·m. The safety factor of the secondary lining varies from 6.7 to 9.7, and the minimum value still appears at No. 7 and No. 8 monitoring

points, indicating that the left and right wall feet are the most unfavorable positions for structural stress, but still greater than the critical threshold, meeting the requirements for tunnel service.

When the temperature decreases in winter, under the action of temperature stress, the tunnel arch of the secondary lining is under pressure, and the arch springs, wall springs, and inverted arch are all under tension. The maximum pressure occurs at No. 1 and No. 2 monitoring points, reaching 15.0 kN, and the maximum tension occurs at No. 7 and No. 8 monitoring points, reaching −31.7 kN; the tunnel vault and inverted arch of the secondary lining bear the positive bending moment, while the arch waist, arch springs, and wall springs bear the negative bending moment. The maximum positive bending moment occurs at No. 11 monitoring point, reaching 137.8 kN·m, and the maximum negative bending moment occurs at No. 7 and No. 8 monitoring points, reaching −70 kN·m. The safety factor of the secondary lining is between 7.4 and 31.7, with the minimum value occurring at the center of the inverted arch, indicating that the center of the inverted arch is the most unfavorable position for structural stress under temperature stress, but it can still meet the safety requirements of the tunnel. Through comparison, it was found that the minimum safety factor of secondary lining under temperature stress is slightly greater than that under self-weight. The minimum safety factor determined by on-site measurement is smaller than that determined by simulation (only bearing temperature stress), which is about 51% of the latter. From this, it can be seen that the effect of temperature stress alone has the smallest impact on the safety of secondary lining compared to self-weight and engineering practice, but it cannot be ignored.

Comparative analysis of the internal force simulation results of secondary lining in summer and winter reveals that:

(1) Whether in winter or summer, the axial force is most pronounced at the arch springs and wall springs of the secondary lining. The maximum positive bending moment in summer and the maximum negative bending moment in winter both occurred at the wall springs, indicating that the wall springs are most significantly affected by temperature stress. The axial force and bending moment of the tunnel arch are relatively small, indicating that the influence of temperature stress on the tunnel arch is relatively gentle.

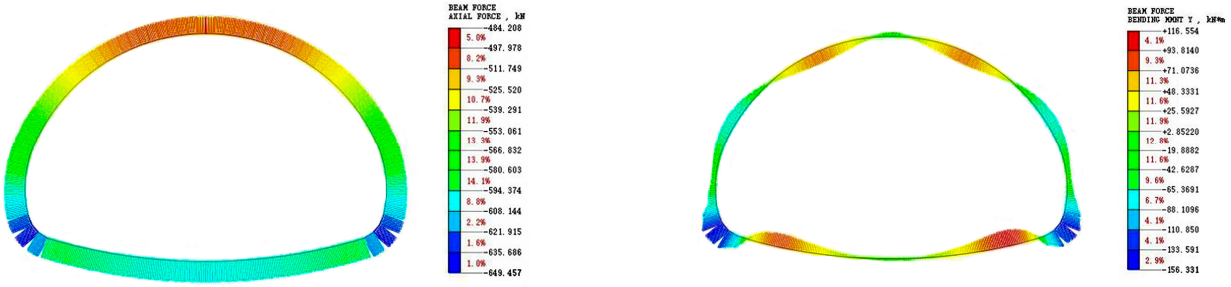
(2) In summer, as the temperature increases, the axial force of the secondary lining increases while the bending moment decreases. In winter, the opposite is true, indicating that for secondary lining, an increase in temperature leads to an increase in axial force, while a decrease in temperature leads to an increase in bending moment.

4.2.3. Mechanical Behavior of Secondary Lining under the Combined Action of Gravity Load and Temperature Stress

When the secondary lining is subjected to both gravity load and temperature stress, the internal force simulation results of the secondary lining are displayed in Figures 22 and 23, and the statistical results of axial force and bending moment values are listed in Table 8.

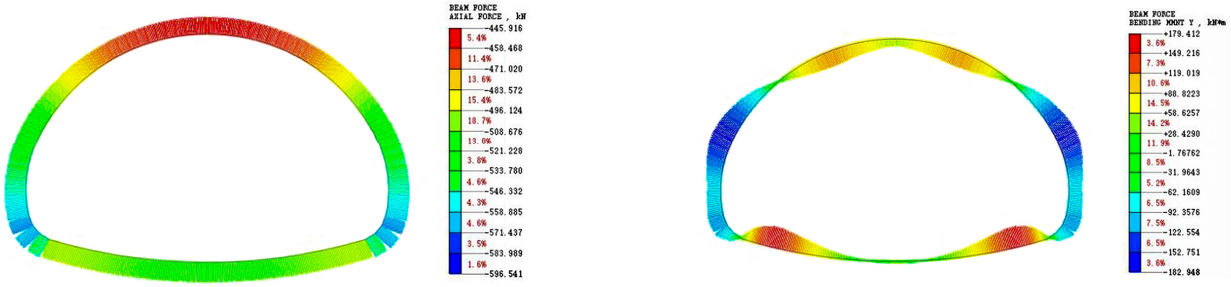
Table 8. Simulation results of internal forces in secondary lining under self-weight and temperature stress.

Seasons	Positions	0	1	2	3	4	5	6	7	8	9	10	11
Self-weight + summer	Axial force (kN)	484.4	497.7	497.7	547.8	547.8	598.1	598.1	629.5	629.5	593.8	593.8	600.7
	Bending moment (kN·m)	26.3	−66.5	−66.5	61.8	61.8	45.6	45.6	110.2	110.2	−69.8	−69.8	7.9
	Safety factor	4.6	3.8	3.8	3.6	3.6	3.5	3.5	2.8	2.8	3.3	3.3	4.0
Self-weight + winter	Axial force (kN)	445.9	464.1	464.1	526.0	526.0	574.5	574.5	584.2	584.2	508.6	508.6	516.4
	Bending moment (kN·m)	−39.7	−112.9	−112.9	117.5	117.5	97.6	97.6	118.0	118.0	−104.3	−104.3	10.0
	Safety factor	5.4	4.3	4.3	4.0	4.0	4.0	4.0	3.8	3.8	4.2	4.2	5.6



(**a**) (**b**)

Figure 22. Internal force of secondary lining under self-weight in summer. (**a**) Axial force. (**b**) Bending moment.



(**a**) (**b**)

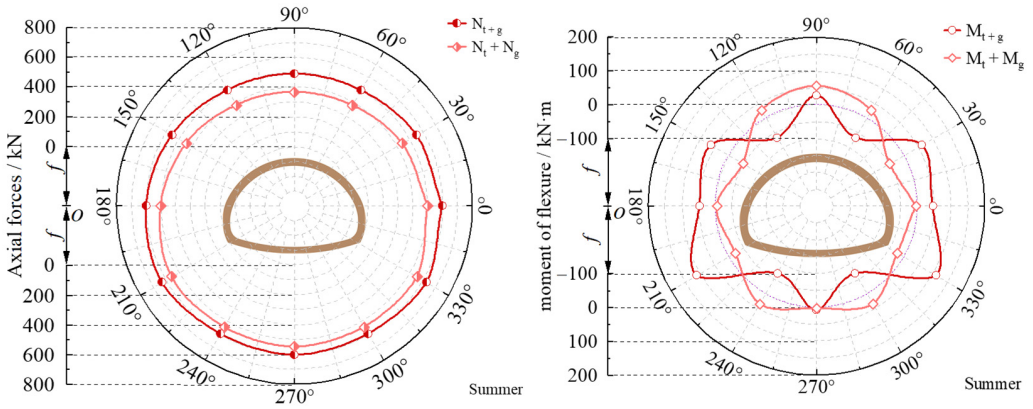
Figure 23. Internal force of secondary lining under self-weight in winter. (**a**) Axial force. (**b**) Bending moment.

According to Table 8 and Figures 22 and 23, it can be seen that under the coupling effect of gravity load and temperature stress, the secondary lining is in a compressed state in summer, with the minimum axial force appearing at the tunnel arch and the maximum axial force appearing at the wall springs, and the maximum axial force reaches 629.5 kN. The arch waist and inverted arch of the secondary lining bear the negative bending moments, while other positions bear the positive bending moments. The maximum positive bending moment occurs at No. 7 and No. 8 monitoring points, reaching 110.2 kN·m, and the maximum negative bending moment occurs at No. 9 and No. 10 monitoring points, reaching −69.8 kN·m. The safety factor of the secondary lining is between 2.8 and 4.6, with the minimum value appearing at the feet of the sidewall. Although the safety factor of the secondary lining is greater than the critical threshold (2.0), it is much lower than the structural safety factors under the individual action of self-weight and temperature stress, indicating that the coupling effect of self-weight and temperature stress intensifies the adverse stress on the lining structure and reduces its safety. In addition, the minimum safety factor of the secondary lining under the combined effect of summer temperature and self-weight accounts for 42% and 48% of the minimum safety factors under temperature stress only and self-weight only, respectively. Compared with the safety factors determined by on-site measurement, it can be seen that the minimum safety factor under the combined effect of summer temperature and self-weight accounts for 82% of that in actual engineering, indicating that the numerical simulation results are very close to the actual engineering.

In winter, under the coupling effect of gravity load and temperature stress, the secondary lining is in a compressed state as a whole, with the minimum axial force occurring at the tunnel arch and the maximum axial force occurring at the wall springs, and the maximum axial force reaches 584.2 kN. The tunnel arch and inverted arch of the secondary lining bear the negative bending moment, while other positions bear the positive bending moment. The maximum positive bending moment appears at No. 7 and No. 8 monitoring points, reaching 118.0 kN·m, and the maximum negative bending moment appears at No. 1 and No. 2 monitoring points, reaching −112.9 kN·m. The safety factor of the secondary

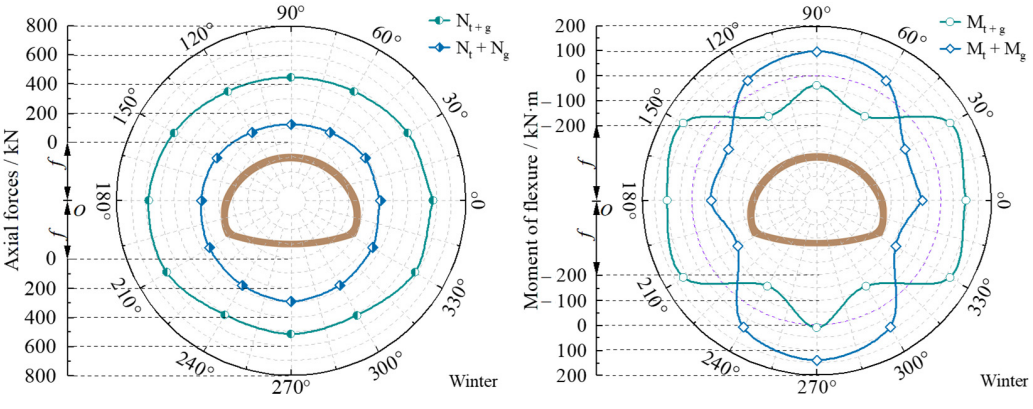
lining ranges from 3.8 to 5.6, slightly greater than the structural safety factor in summer, but also much lower than the safety factor under the individual action of self-weight and temperature stress, indicating that the coupling effect of self-weight and temperature stress in both summer and winter has a significant adverse effect on the stress and safety of the secondary lining. In addition, the minimum safety factor of the secondary lining under the combined effect of winter temperature and self-weight accounts for 51% and 65% of the minimum safety factors under temperature stress only and self-weight only, respectively. Compared with the safety factors determined by on-site measurement, it can be seen that the minimum safety factor under the combined effect of summer temperature and self-weight accounts for 83% of that in actual engineering, indicating that the numerical simulation results are very close to the actual engineering.

For the convenience of analyzing the influence of temperature and gravity on the internal force of the secondary lining, the axial force and bending moment generated by temperature on the secondary lining are denoted as N_t and M_t, respectively. The axial force and bending moment generated by gravity are denoted as N_g and M_g, respectively. The axial force and bending moment generated by the coupling effect of gravity and temperature are denoted as N_{t+g} and M_{t+g}, respectively. The axial force and bending moment of the secondary lining under different working conditions in summer and winter are illustrated in Figures 24 and 25.



(**a**) (**b**)

Figure 24. Comparison of axial force and bending moment of secondary lining under different working conditions. (**a**) Axial force. (**b**) Bending moment.



(**a**) (**b**)

Figure 25. Comparison of axial force and bending moment of secondary lining under different working conditions. (**a**) Axial force. (**b**) Bending moment.

From Figures 24 and 25, it can be seen that the average value of the sum of axial forces (N_t + N_g) at different locations of the secondary lining in winter is 210 kN, and

the average value in summer is 476 kN, which is 266 kN higher than that in winter. The reason for this is that as the temperature increases in summer, the secondary lining undergoes volume expansion, which is constrained by the outer surrounding rock and primary support. The secondary lining cannot expand and deforms radially towards the direction of the surrounding rock, and the circumferential compression force in the cross-section of the secondary lining increases, resulting in an increase in axial force. In addition, the average N_{t+g} in winter reaches 523 kN, which is 313 kN greater than the average $N_t + N_g$ in winter. The average N_{t+g} in summer reaches 568 kN, which is 302 kN greater than the average $N_t + N_g$ in summer. The maximum value of the superimposed bending moments ($M_t + M_g$) in summer is 55.5 kN·m, and the maximum value of M_{t+g} in summer is 110.2 kN·m. The maximum value of the superimposed bending moments ($M_t + M_g$) in winter is 57.0 kN·m, and the maximum value of M_{t+g} in winter is 118.0 kN·m. The superimposed bending moments ($M_t + M_g$) in summer and winter are smaller than the bending moments M_{t+g} generated by the combined effects of temperature stress and self-weight, with the former only being about half of the latter. The distribution patterns of superimposed bending moments ($M_t + M_g$) in winter and summer are similar. The superimposed bending moments ($M_t + M_g$) at the tunnel vault and inverted arch are positive, and the superimposed bending moments ($M_t + M_g$) at the arch waist, arch feet and wall feet are negative. The M_{t+g} is negative at the tunnel vault and inverted arch and is positive at the arch waist, arch springs and wall springs positions. This is different from the superposition of internal forces under the separate action of the two factors. The analysis suggests that it is mainly caused by two reasons. Firstly, due to the low stress of concrete, there is a phenomenon of tension−compression transition with temperature changes in winter and summer. Secondly, the gradient change of temperature in the radial direction of the secondary lining was ignored in the numerical simulation, and it was assumed that the influence of temperature stress on the inner and outer sides of the lining section was consistent. Under the coupling effect of self-weight and temperature stress, there is an eccentric compression−tension phenomenon in the secondary lining section, which is significantly different from the superposition of internal force under the individual action of the two factors. It is evident that the axial force and bending moment of the secondary lining are the result of the coupling effect of temperature and gravity, rather than the superposition of the effects of temperature and gravity alone.

5. Conclusions

Based on finite element numerical analysis and on-site testing of the Letuan Tunnel, this paper investigates the stress properties of the secondary lining of a double-hole eight-lane large-span highway tunnel under periodic temperature changes. The main conclusions include:

(1) Field test results show that the stress of secondary lining steel bars and concrete is greatly affected by seasonal temperature differences. Specifically, the compressive stress of secondary lining steel bars and concrete is significantly greater in summer than in winter, while the tensile stress is greater than in winter. In summer, the phenomenon of tension and compression stress state conversion occurred at many monitoring points.

(2) The stress values of steel bars and concrete fluctuate periodically as a sinusoidal function over time. The overall pattern shows an increase as the temperature increases in summer and decreases as the temperature decreases in winter. The fluctuation period is one year.

(3) The fluctuation amplitude of the concrete and steel stress on the inside of the secondary lining is greater than that on the outside. Among them, the amplitude of the flat fluctuation of stress at each monitoring point on the outside of the concrete with time is between 0.44 and 1.07 MPa; the amplitude on the inside of the concrete is between 0.77 and 1.75 MPa; The amplitude of the stress of the outer steel bars is between 7 and 13 MPa; the amplitude of the inner steel bars is between 5 and 31 MPa. The safety

factor in summer is smaller than that in winter. The minimum safety factors of the secondary lining in summer and winter are 3.4 and 4.6, respectively.

(4) The axial force and bending moment of the secondary lining arch are small, and the maximum axial force and bending moment appear at the springs of the wall. The average axial force of the secondary lining under the coupled effects of self-weight and temperature in winter and summer is 528 MPa and 563 MPa, respectively, which is significantly greater than the superposition of the axial forces under the separate effects of the two. The bending moment distribution at the arch, wall base and other positions is different from the superposition of bending moments under the separate action of the two. It is even opposite, indicating that the influence of temperature stress on the internal force of the lining structure cannot be ignored, and the influence of self-weight and temperature coupling on the internal force of the lining structure is far away. It is more complex than the superposition of the two acting alone.

Author Contributions: Conceptualization, Y.L. (Yanbin Luo) and J.C.; methodology, Y.L. (Yanbin Luo) and F.D.; software, Y.L. (Yahui Liu); validation, Y.L. (Yanbin Luo), C.W. and Y.L. (Yahui Liu); formal analysis, F.D. and Y.L. (Yanbin Luo); investigation, F.D., Y.L. (Yahui Liu) and W.X.; resources, Y.L. (Yanbin Luo), J.C. and Y.L.; data curation, Y.L. (Yahui Liu) and C.W.; writing—original draft preparation, F.D.; writing—review and editing, F.D. and W.X.; visualization, Y.L. (Yahui Liu) and W.X.; supervision, J.C.; project administration, J.C.; funding acquisition, J.C. All authors have read and agreed to the published version of the manuscript.

Funding: This research was funded by the National Natural Science Foundation of China, grant numbers 51978065 and 52278394.

Data Availability Statement: The data that supports the findings of this study are available within the manuscript.

Conflicts of Interest: Author Yahui Liu was employed by the company Guangzhou Metro Design & Research Institute Co., Ltd. The remaining authors declare that the research was conducted in the absence of any commercial or financial relationships that could be construed as a potential conflict of interest.

References

1. He, M.C.; Guo, A.P.; Du, Z.F.; Liu, S.Y.; Zhu, C.; Cao, S.D.; Tao, Z.G. Model test of negative Poisson's ratio cable for supporting super-large-span tunnel using excavation compensation method. *J. Rock. Mech. Geotech.* **2023**, *15*, 1355–1369. [CrossRef]
2. Liu, C.; Li, S.C.; Zhou, Z.Q.; Li, L.P.; Wang, K.; Qin, C.S. Model test study on spatial deformation law of surrounding rock for super-large section and shallow buried tunnels. *Geotech. Test. J.* **2019**, *42*, 703–724. [CrossRef]
3. Zhao, J.P.; Tan, Z.S.; Yu, R.S.; Li, Z.L.; Wang, X.Y. Mechanical responses of a shallow-buried super-large-section tunnel in weak surrounding rock: A case study in guizhou. *Tunn. Undergr. Sp. Technol.* **2023**, *131*, 104850. [CrossRef]
4. Ministry of Transport of the People's Republic of China. *Design Rules for Highway Tunnels: JTG/T D70-2010*; China Communication Press: Beijing, China, 2010.
5. Liu, W.W.; Chen, J.X.; Chen, L.J.; Luo, Y.B.; Shang, Q.C.; Zhang, L.X.; Gao, S.K.; Jia, H.Y. A rational construction method and deformation control system of tunnelling in extremely soft and fractured chlorite schist medium. *Tunn. Undergr. Sp. Technol.* **2024**, *143*, 105472. [CrossRef]
6. Pu, C.P.; Xia, C.C.; Li, Y.S.; Weng, X.N. Study of thermo-stress of highway tunnel and the law of line-fissure development caused by the thermo-stress. *China J. Highw. Transp.* **2000**, *2*, 78–81.
7. Xu, Z.L.; Chen, J.X.; Luo, Y.B.; Zhu, H.Y.; Liu, W.W.; Shi, Z.; Song, Z.G. Geomechanical model test for mechanical properties and cracking features of Large-section tunnel lining under periodic temperature. *Tunn. Undergr. Sp. Technol.* **2022**, *123*, 104319. [CrossRef]
8. Li, P.F.; Zhao, Y. Performance of a multi-face tunnel excavated in loess ground based on field monitoring and numerical modeling. *Arab. J. Geosci.* **2016**, *9*, 1–10. [CrossRef]
9. He, B.G.; Zhu, Y.Q.; Sun, M.L.; Liu, H.Y.; Zhang, Z.Q. In situ experiments on supporting load effect of large span deep tunnels in hard rock. *J. Mt. Sci. Engl.* **2013**, *10*, 1125–1136. [CrossRef]
10. Xu, G.W.; He, C.; Wang, J.; Chen, Z.Q. Study on the Mechanical Behavior of a Secondary Tunnel Lining with a Yielding Layer in Transversely Isotropic Rock Stratum. *Rock. Mech. Rock. Eng.* **2020**, *53*, 2957–2979. [CrossRef]
11. Tan, Z.S.; Zhou, Z.L.; Kong, H.; Zhao, B.J.; Zhao, J.P. Single excavation face method for super-large-span bifurcated tunnels, P.I. *Civil. Eng. Geotec.* **2021**, *174*, 406–418.

12. He, J.X.; He, S.H.; Liu, X.B.; Ma, J.F.; Li, Y.M.; Zhang, B. Investigating the mechanical responses and construction optimization for shallow super-large span tunnels in weathered tuff stratum based on field monitoring and flac3d modeling. *Int. J. Civ. Eng.* **2023**, *22*, 379–395. [CrossRef]
13. Mostafa, S.; Farshad, K.; Masoud, G.; Shahaboddin, Y. Design of sequential excavation method for large span urban tunnels in soft ground—Niayesh tunnel. *Tunn. Undergr. Sp. Technol.* **2013**, *35*, 178–188.
14. He, J.X.; He, S.H.; Liu, X.B.; Zheng, J.L. Structural design and mechanical responses of closely spaced super-span double tunnels in strongly weathered tuff strata. *Front. Struct. Civ. Eng.* **2022**, *16*, 685–703. [CrossRef]
15. Liu, D.P.; Zhang, D.L.; Fang, Q.; Sun, Z.Y.; Luo, J.W.; Li, A. Field monitoring of the deformation and internal forces of the surrounding rock and support structures in the construction of a super-span high-speed railway tunnel—A case study. *Appl. Sci.* **2020**, *10*, 5182. [CrossRef]
16. Zhou, S.; Li, L.P.; An, Z.M.; Li, H.L.; Yang, G.Y.; Zhou, P.F. Stress-release law and deformation characteristics of large-span tunnel excavated with semi central diaphragm method. *KSCE J. Civ. Eng.* **2021**, *25*, 2275–2284. [CrossRef]
17. Li, L.P.; Shang, C.S.; Chu, K.W.; Zhou, Z.Q.; Song, S.G.; Liu, Z.H.; Chen, Y.H. Large-scale geo-mechanical model tests for stability assessment of super-large cross-section tunnel. *Tunn. Undergr. Sp. Technol.* **2021**, *109*, 103756. [CrossRef]
18. Zhang, J.R.; Wang, Z.Y.; Feng, J.M.; Yu, L.P.; Zhou, P.; Li, Z.L. Deformation control for large-section tunnel construction in fractured carbonaceous slate, P.I. *Civil. Eng. Geotec.* **2021**, *176*, 132–145. [CrossRef]
19. Li, P.F.; Zhang, D.L.; Zhao, Y.; Zhou, Y.; Fang, Q.; Zhang, X. Study of mechanical characteristics of secondary lining of large-section loess tunnel. *Chin. J. Rock Mech. Eng.* **2010**, *29*, 1690–1696.
20. Fang, Y.; Xu, C.; Chen, X.G.; Guo, J.N. Scaled model test on mechanical characteristics of large cross-section highway tunnel lining under water pressure. *China Civ. Eng. J.* **2016**, *49*, 111–119.
21. Wu, C.; Huang, L.; Chen, Z.T.; Fang, Y. Model Test for Mechanical Characteristics of Secondary Lining of Large Cross-section Highway Tunnel. *Tunn. Constr.* **2018**, *38*, 977–985.
22. Zhao, P.Y.; Chen, J.X.; Luo, Y.B.; Li, Y.; Chen, L.J.; Wang, C.W.; Hu, T.T. Field measurement of air temperature in a cold region tunnel in northeast China. *Cold Reg. Sci. Technol.* **2020**, *171*, 102957. [CrossRef]
23. Zhang, S.C.; Chen, W.H.; Liu, H. Dynamic Response of Tunnels Surrounded by Thawing Permafrost with Anisotropic Frost Heave in Cold Regions: Considering the Movement of the Frozen Interface. *J. Eng. Mech.* **2023**, *149*, 04022112. [CrossRef]
24. Ling, X.Z.; Yu, Y.; Tang, L.; Geng, L.; Han, X. The lining responses for shallow mountain tunnels subjected to frost heaving. *J. Mt. Sci.* **2022**, *19*, 529–546. [CrossRef]
25. Li, H.W.; Lai, Y.; Zhang, H.Y.; Chen, Y.Y.; Jiang, W.T.; Tian, Y.; Ran, J.C. Composite lining-ground interaction behavior in a cold-region circular tunnel under isotropic frost heave action. *Cold Reg. Sci. Technol.* **2023**, *207*, 103771. [CrossRef]
26. Li, H.W.; Lai, Y.; Zhang, H.Y.; Chen, Y.Y.; Jiang, W.T.; Ran, J.C. Composite lining-ground interaction behavior in a cold-region circular tunnel under anisotropic frost action. *Int. J. Rock Mech. Min. Sci.* **2023**, *164*, 105341. [CrossRef]
27. Xu, P.; Wu, Y.M.; Huang, L.; Zhang, K. Study on the progressive deterioration of tunnel lining structures in cold regions experiencing freeze–thaw cycles. *Appl. Sci.* **2021**, *11*, 5903. [CrossRef]
28. Sutoh, A.; Maruyama, O.; Kanekiyo, H.T.; Sato, T. A Consideration on Deterioration Model for Cold Region Tunnel Lining Based on Life-cycle Concept. *Geotech. Saf. Risk V.* **2015**, 413–418. [CrossRef]
29. Zhao, X.; Zhang, H.W.; Lai, H.P.; Yang, X.H.; Wang, X.Y.; Zhao, X.L. Temperature field characteristics and influencing factors on frost depth of a highway tunnel in a cold region. *Cold Reg. Sci. Technol.* **2020**, *179*, 103141. [CrossRef]
30. Yang, J.; Wang, T.; He, X.; Su, Y.; Dai, F.; Xiong, L.; Zhao, R.; Duan, X. Preparation and Experimental Investigations of Low-Shrinkage Commercial Concrete for Tunnel Annular Secondary Lining Engineering. *Materials* **2022**, *15*, 6848. [CrossRef]
31. Ministry of Transport of the People's Republic of China. *Specifications for Design of Highway Tunnels: JTG 3370.1-2018*; China Communication Press: Beijing, China, 2018.
32. Fairbairn, E.M.R.; Silvoso, M.M.; Toledo Filho, R.D.; Alves, J.L.D.; Ebecken, N.F.F. Optimization of mass concrete construction using genetic algorithms. *Comput. Struct.* **2004**, *82*, 281–299. [CrossRef]

Disclaimer/Publisher's Note: The statements, opinions and data contained in all publications are solely those of the individual author(s) and contributor(s) and not of MDPI and/or the editor(s). MDPI and/or the editor(s) disclaim responsibility for any injury to people or property resulting from any ideas, methods, instructions or products referred to in the content.